N. Corona, M. Porru and A. Serpi, "A Rule-based Energy Management System for a Marine Electric Propulsion System," 2025 IEEE Vehicle Power and Propulsion Conference (VPPC), Hangzhou, China, 2025, pp. 1-5.

The publisher's version is available at:

http://dx.doi.org/10.1109/VPPC66000.2025.11393003

A Rule-based Energy Management System for a Marine Electric Propulsion System

Nicola Corona, Mario Porru, Alessandro Serpi
Department of Electrical and Electronic Engineering
University of Cagliari
Cagliari, Italy

***Abstract*—This paper proposes a rule-based Energy Management System (EMS) for the marine electric propulsion system presented by the IEEE Motor Vehicle Challenge (MVC) 2025. The system integrates a Dual Three-Phase Permanent Magnet Synchronous Machine (DTP-PMSM), whose three-phase windings are supplied by a battery pack and a supercapacitor module, respectively. The proposed EMS optimizes the DTP-PMSM power flow by utilizing the supercapacitor module to compensate for sudden power variation, by providing peak shaving during towing operations as well. Simulations based on the IEEE MVC 2025 reference cycles demonstrate effective power distribution and reduced battery current fluctuations achievable by the proposed EMS compared to the MVC 2025 baseline EMS.**

Keywords—Batteries, Electric propulsion systems, Energy management systems, Supercapacitors

I. Introduction

The maritime industry is experiencing a significant transformation in order to mitigate its environmental impact and comply with increasingly stringent emissions regulations. While the global maritime sector accounts for only a marginal part of total greenhouse gas emissions, the shift toward cleaner propulsion systems has become a priority. Particularly, hybrid-electric and full Electric Propulsion Systems (EPSs) are emerging as viable alternatives to traditional diesel engines, offering lower emissions, reduced fuel consumption, and enhanced flexibility.

A key challenge in the electrification of marine propulsion system is managing the highly variable power demands of vessels, which range from steady-state low-power requirements (e.g. cruising) to sudden and short high-power demands (e.g. manoeuvres). Battery energy storage systems are capable to provide power for propulsion and auxiliary loads, while they are effective also in peak shaving and rapid load response in hybrid configurations, especially in short-range vessels [1]. However, battery-only systems face issues due to frequent and deep charging/discharging cycles and sudden current variations, leading to accelerated battery degradation and reduced lifespan [2]. To cope with these issues and address operating efficiency and fluctuating power demands, marine EPSs are increasingly integrating Hybrid Energy Storage Systems (HESS), typically combining batteries and supercapacitors. Consequently, Energy Management Systems (EMSs) play a crucial role in optimising the overall EPS performance, at both design stage and under variable operating conditions.

The EMSs can be roughly classified into three main groups: Rule-Based (RB-EMSs), Optimisation-Based (OB-EMSs) and Artificial Intelligence-based EMSs (AI-EMSs) [3], [4], [5], [6], [7], [8]. RB-EMSs employ predefined set of rules or logic to split power between the different energy storage systems. The power split criterion is generally based on system state and operating conditions, such as battery state-of-charge and load power demand, and human expertise is required to set up rules and tune up parameters. RB-EMSs are simple, easy to implement, and suitable for real-time applications, but they may not achieve optimal performance under all operating conditions. [3] Alternatively, OB-EMSs use mathematical models in order to find the optimum of a given objective function and achieve one or multiple specific goals, such as minimum fuel consumption or reduced battery degradation. Finding an optimal solution comes at the cost of higher complexity and lower real-time feasibility, when compared to RB-EMS [4], [5], [6]. The AI-EMSs resort to machine learning to derive the optimal control laws by employing massive historical and real-time information. Even if they are easy to implement in real-time, setup a correct database is difficult and time-consuming, and structure and size of database directly affect system performance. Hence, AI-EMSs also employ AI techniques to adjust control parameters of conventional EMSs based on real-time feedback of the vessel and/or energy storage systems [7], [8].

In this context, this paper proposes an RB-EMS for the marine EPS equipped with an HESS promoted by the IEEE Motor Vehicle Challenge (MVC) 2025 [9], [10]. Particularly, the EPS propels an electric tugboat, and consists of a Dual Three Phase Permanent Magnet Synchronous Machine (DTP-PMSM), whose three-phase windings are supplied by a Battery Pack (BP) and a Supercapacitor Module (SM) through dedicated DC/DC and DC/AC converters. The vessel speed is regulated through motor speed and current control loops, while torque and current distribution among the DTP-PMSM windings can be unbalanced by the EMS to regulate the power flow among BP, SM, and DTP-PMSM. The EMS proposed in this paper has been designed to accomplish several goals; first, SM should support BP over fast torque/power variations. Second, SM should smooth high-power peaks that occur during towing operation, relieving BP high currents. Third, the EMS must reinstate SM energy content during medium and long time intervals. Several simulations that refer to the case studies provided by the IEEE MVC 2025 reveal the effectiveness of the proposed EMS compared to the baseline EMS provided by the competition.

II. System Modelling

A simplified view of the EPS under study is shown in Fig. 1, whose details can be found in [9], [10]. The powertrain consists of two independent energy sources, i.e. a BP and an SM, each of which supplies one of the two three-phase windings of the DTP-PMSM through appropriate DC-DC and DC/AC converters. The DTP-PMSM shaft is connected to a fixed-pitch marine propeller through a gearbox.

A. Mechanical Powertrain

Vessel speed (v) can be controlled in accordance with:

$$F_p = M\frac{dv}{dt}+F_r\ ,\quad F_r=\sigma_v f\,\frac{1}{2}\rho S_v v^2 \tag{1}$$

in which F_p is the thrust force, M is the vessel mass, an F_r is the resistance force. The latter depends on water mass density

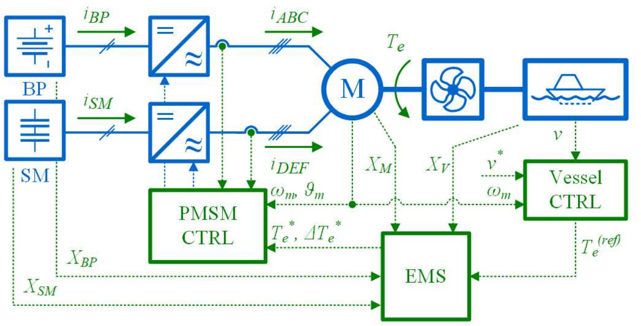

Fig. 1. The EPS under study, in which X_Y denotes the state/output variables of the system Y.

ρ, on f, which is a dimensional-less coefficient depending on the Froude's number, and on the vessel wetted area (S_v) [11]. On the other hand, F_p depends on propeller torque T_p as

$$F_P = \frac{k_F}{k_T}\frac{T_p}{D_P}, \quad T_p = \sigma_\omega k_T \rho D_p^5 \left(\frac{\omega_p}{2\pi}\right)^2 \tag{2}$$

where k_T and k_F are the torque and the thrust coefficient, respectively, D_p is the propeller diameter, and σ_ω is the sign of the propeller speed (ω_p).

Considering the torque balance at the DTP-PMSM shaft, the following equation holds:

$$T_e = J\frac{d\omega_m}{dt} + D\omega_m + T_L \tag{3}$$

in which J and D represent the inertia and the damping coefficient, respectively, while T_L is the load torque that is proportional to T_p through the gear ratio g:

$$T_L = \frac{T_p}{g}, \quad \omega_p = \frac{\omega_m}{g}. \tag{4}$$

B. Electrical powertrain

The DTP-PMSM can be modelled in terms of space vectors in the stationary reference frame (αβxy0z) by the following equations [10]:

$$\begin{aligned} v_{\alpha\beta} &= r\,i_{\alpha\beta} + L_s\frac{di_{\alpha\beta}}{dt} + 2j\omega\Lambda e^{j\vartheta} \\ v_{xy} &= r\,i_{xy} + L_0\frac{di_{xy}}{dt}, \quad v_{0z} = r\,i_{0z} + L_0\frac{di_{0z}}{dt} \end{aligned} \tag{5}$$

in which v and i are voltage and current space vectors, respectively, r is the phase winding resistance, L_s and L_0 are the synchronous and the zero-sequence inductance, respectively, and Λ denotes the equivalent magnetic flux linkage magnitude due to PM. Additionally, ϑ and ω are electric rotor position and speed, which are proportional to mechanical position and speed (ω_m) through the number of poles pairs (p).

Assuming no zero-sequence current component, moving from the αβ (xy) to the dq+ (dq–) reference frame yields [10]

$$\begin{aligned} v_{dq+} &= \left(r + j\omega L_s\right) i_{dq+} + L_s\frac{di_{dq+}}{dt} + 2j\omega\Lambda \\ v_{dq-} &= \left(r - j\omega L_0\right) i_{dq-} + L_0\frac{di_{dq-}}{dt}. \end{aligned} \tag{6}$$

Consequently, given the ⅔ coefficient used in defining the αβ and xy space vectors [10], the electromagnetic power and power unbalance can be achieved as:

$$P_m = \frac{3}{2}\omega\Lambda i_{q+}, \quad \Delta P_m = \frac{3}{2}\omega\Lambda i_{q-}. \tag{7}$$

Focusing on (7), P_m accounts for the overall electromagnetic power coming from the two DTP-PMSM three-phase windings (ABC and DEF), whereas ΔP_m quantifies the additional electromagnetic power/torque provided by the winding DEF compared to ABC (positive values). Therefore, electromagnetic torque and its unbalance can be achieved easily by diving (7) by ω_m, leading to

$$T_e = \frac{3}{2}p\Lambda i_{q+}, \quad \Delta T_e = \frac{3}{2}p\Lambda i_{q-}. \tag{8}$$

Considering the overall electrical power balance, the following relationships hold:

$$P_X = P_m^{(X)} + \Delta P^{(X)}, \quad X \in \{BP, SM\} \tag{9}$$

in which P_X denotes the power delivered or drawn by BP or SM, while $P_m^{(X)}$ and $\Delta P^{(X)}$ are the corresponding contributions to the overall electromagnetic power demand (P_m) and losses (ΔP), respectively. Consequently, summing (9) to each other yields

$$P_{BP} + P_{SM} = P_m + \Delta P, \quad P_{SM} = -\frac{dE_{SM}}{dt} \tag{10}$$

where E_{SM} denotes the SM energy content.

III. Energy Management System

A. Cost function

The EMS should be developed to minimise the following cost function over a certain time horizon T [9]:

$$\Phi = k_{BP}\phi_{BP} + k_E\phi_E + k_{SPM}\phi_{SPM} + k_w\phi_w \tag{11}$$

in which:

$$\phi_{BP}^2 = \frac{1}{T}\int_T \left(\frac{di_{BP}}{dt}\right)^2 dt, \quad \phi_E = \left(E_{BP} + E_{SM}\right)\Big|_T^0 \tag{12}$$

$$\phi_{SPM} = \frac{1}{T}\int_T \sum_h \left(P_{m,h}^2 - \left(\gamma P_{m,n}\right)^2\right)\Big\rangle_0^{+\infty} dt, \quad x\big\rangle_0^{+\infty} = max\{x,0\} \tag{13}$$

$$\phi_w = \frac{1}{T}\int_T \left(1\big|_{\|i_{ABC}\|=0} + 1\big|_{\|i_{DEF}\|=0}\right)\frac{|T_e^*|}{T_{e,n}} dt, \quad 1\big|_{x=0} = \begin{cases} 1 & if\ \ x = 0 \\ 0 & o/w \end{cases} \tag{14}$$

while the weighting coefficients k_{BP}, k_E , k_{SPM}, and k_w make all the ϕ terms consistent to each other. Considering ϕ_{BP} at first, it penalizes BP current (i_{BP}) fluctuations, especially when they occur at high time rates, while ϕ_E accounts for the overall energy usage, E_{BP} being the BP energy content. Regarding ϕ_{SPM}, this term aims at penalizing an excessive power unbalance between the two DTP-PMSM phase windings. Particularly, when either $P_{m,ABC}$ or $P_{m,DEF}$ exceeds $\gamma P_{m,n}$ (with $0 < \gamma < 1$), in which $P_{m,n}$ denotes the rated electromagnetic power, positive ϕ_{SPM} values occur. Otherwise, ϕ_{SPM} is nullified. On the other hand, ϕ_w accounts for a weak exploitation of each DTP-PMSM winding, $\|i_{ABC}\|$ and $\|i_{DEF}\|$ denoting the magnitude of the two three-phase current sets, while T_e^* and $T_{e,n}$ are the reference and rated torque, respectively. In other words, both windings should operate simultaneously if any DTP-PMSM torque is required.

B. Proposed EMS

Starting from (10) and assuming a given reference electromagnetic power profile (P_m^*), the EMS should determine the most suitable reference BP and SM power profiles to achieve a multi-objective optimisation. In particular, SM should support BP over dynamic operation, but

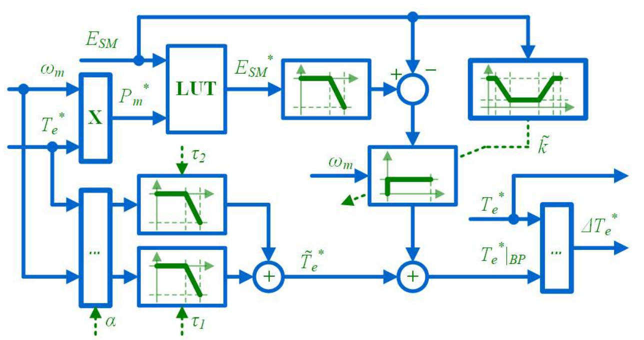

Fig. 2. The proposed EMS, in which $\omega_m \in X_M$ and $E_{SM} \in X_{SM}$.

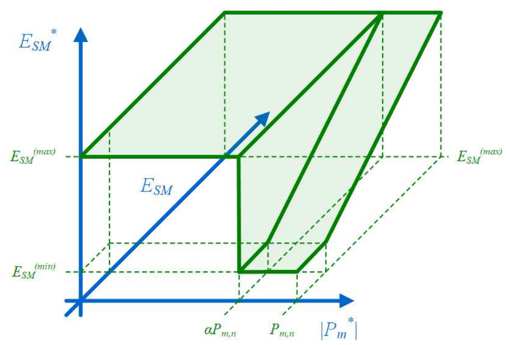

Fig. 3. The E_{SM}^* map as a function of P_m^* and E_{SM}.

it should also prevent BP from handling high-power demand in the medium term. Given these considerations, (10) can be expressed as

$$\frac{dE_{SM}}{dt} = P_{BP} - P_m^* - \Delta P \,. \tag{15}$$

Since SM should not be fully charged or discharged suddenly, which would force P_{BP} to vary abruptly, (15) suggests defining P_{BP}^* so that E_{SM} can track a suitable reference profile (E_{SM}^*). Consequently, the following expression can be considered:

$$P_{BP}^* = P_m^* + k\left(E_{SM}^* - E_{SM}\right). \tag{16}$$

Assuming $P_{BP} = P_{BP}^*$, substituting (16) into (15) yields

$$\frac{dE_{SM}}{dt} + kE_{SM} = kE_{SM}^* - \Delta P \,. \tag{17}$$

Applying the Laplace's transformation to (17) results in

$$E_{SM} = \frac{k}{s+k}E_{SM}^* + \frac{1}{s+k}\Delta P \tag{18}$$

in which s denotes the Laplace's variable, while all the other variables are intended expressed in the s domain. Consequently, (17)-(18) ensure that E_{SM} tracks E_{SM}^* with the desired dynamic performance imposed by k.

However, setting P_{BP}^* in accordance with (16) introduces some drawbacks. First, a steady-state error on E_{SM} always occurs because ΔP always differs from zero; this cannot be included in (16) as ΔP is difficult to estimate accurately. This drawback is indeed not very significant as a perfect E_{SM}^* tracking is not required. Much more important is instead the second drawback, namely any sudden variation of P_m^* and/or E_{SM}^* spreads to P_{BP}^* directly, exposing BP to sudden power/current variations. This can be avoided by low-pass filtering both these signals, thus modifying (16) as follows:

$$P_{BP}^* = \frac{1}{1+\tau_1 s}P_m^* + \frac{k}{1+\tau_1 s}E_{SM}^* - kE_{SM} \,. \tag{19}$$

Consequently, applying the Laplace's transformation to (15) and substituting (19) yields

$$E_{SM} = \frac{k}{s+k}\cdot\frac{1}{1+\tau_1 s}E_{SM}^* - \frac{1}{s+k}\cdot\frac{\tau_1 s}{1+\tau_1 s}P_m^* - \frac{1}{s+k}\Delta P \,. \tag{20}$$

Comparing (20) to (18), it can be seen that the E_{SM} steady-state value is the same in both cases, as expected. The most important differences occur over dynamic operations, namely E_{SM} is now transiently affected by P_m^*. In addition, E_{SM} variations with E_{SM}^* and P_m^* share the same dynamic performance, which now depend not only on k, but also on τ_1.

Although (19) overcomes the main drawback of (16), by preventing BP from handling sudden power variations due to E_{SM}^* and/or P_m^*, this equation does not ensure any peak-shaving capability. In other words, SM acts over dynamic operation only as both time constants ($1/k$ and τ_1) are relatively small. Consequently, (19) can be modified as follows

$$P_{BP}^* = \tilde{P}_m^* + \frac{k}{1+\tau_1 s}E_{SM}^* - kE_{SM} \tag{21}$$

in which:

$$\tilde{P}_m^* = \begin{cases} \sigma_m^*\left(\dfrac{\alpha P_{m,n}}{1+\tau_1 s} + \dfrac{\left|P_m^*\right| - \alpha P_{m,n}}{1+\tau_2 s}\right) & if \quad \left|P_m^*\right| > \alpha P_{m,n} \\ \dfrac{P_m^*}{1+\tau_1 s} & o/w \end{cases} \tag{22}$$

where σ_m^* denotes the sign of P_m^*. In particular, if P_m^* overcomes a given threshold ($\alpha P_{m,n}$, $\alpha \in [0,1]$), the overall filtering on P_m^* is split into two complementary actions; the first one still depends on τ_1, but its contribution is bounded at $\pm\alpha P_{m,n}$. The second action depends on another time constant τ_2, which should be much greater than τ_1 to ensure an appropriate peak-shaving capability. As a result, given any P_m^*, (21) enables BP to provide up to $\pm\alpha P_{m,n}$ in a relatively small time, while the residual power is slowly achieved in the medium term in accordance with τ_2. It is worth noting that the greater the time constant τ_2 and the lower the coefficient α, the better the peak-shaving action, but on condition that SM is not fully discharged. Consequently, both α and τ_2 should be set properly in accordance with SM energy capability.

The overall block diagram of the proposed EMS is depicted in Fig. 2. Particularly, (21) has been replaced with the following equation:

$$T_e^*\big|_{BP} = \tilde{T}_e^* + \tilde{k}\frac{\sigma_\omega}{\omega_{m,n}}\left(\frac{1}{1+\tau_1 s}E_{SM}^* - E_{SM}\right) \tag{23}$$

in which

$$\tilde{T}_e^* = \begin{cases} \dfrac{\sigma_e^*}{\left|\omega_m\right|}\left(\dfrac{\alpha P_{m,n}}{1+\tau_1 s} + \dfrac{\left|P_m^*\right| - \alpha P_{m,n}}{1+\tau_2 s}\right) & if \quad \left|P_m^*\right| > \alpha P_{m,nom} \\ \dfrac{T_e^*}{1+\tau_1 s} & o/w \end{cases} \tag{24}$$

where $\omega_{m,n}$ denotes the rated speed, and σ_e^* is the sign T_e^*. This change is required because no power exchange between BP and SM can occur when ω_m is zero. Consequently, implementing (21) leads to BP and SM power dips/spikes when ω_m approaches zero, which should be avoided.

TABLE I PROPOSED EMS PARAMETERS

Parameter	Unit	Value
τ_1	s	1.5461
τ_2	s	13.3991
$\tilde{k}$	s^{-1}	0.32-0.64
α	pu	0.8
E_{SM}^{min}	J	$0.1 \cdot E_{SM,n}$
E_{SM}^{max}	J	$0.9 \cdot E_{SM,n}$

Given (23), E_{SM}^* can be set by a Look-Up Table (LUT), whose graphical representation is depicted in Fig. 3. This figure reveals that E_{SM}^* mostly depends on $|P_m^*|$, namely if this variable is lower than the peak shaving threshold ($\alpha P_{m,n}$), E_{SM}^* is set constant at its maximum value for any E_{SM}. This is because SM should be generally fully recharged at steady-state operation to assist BP in upcoming dynamic operations. Differently, when $|P_m^*|$ overcomes $\alpha P_{m,n}$, E_{SM}^* is set at E_{SM}, thus deactivating the E_{SM} energy recovery. Otherwise, the peak shaving action would be negatively affected by the SM recharging task. The latter is generally regulated by a variable $\tilde{k}$, whose value can be set in accordance with E_{SM} by another LUT; particularly, when E_{SM} approaches it minimum or maximum value, $\tilde{k}$ is relatively high to prevent SM from violating its energy constraint. Otherwise, $\tilde{k}$ could be reduced to recharge SM more slowly. It is worth noting that SM recharging always occurs in case E_{SM} drops at its minimum value, even during peak-shaving, thus preventing any unfeasible SM energy content.

IV. SIMULATIONS

The effectiveness of the proposed EMS has been validated through simulations carried out in MATLAB-Simulink, considering the four reference speed and operating profiles defined by the IEEE MVC 2025 (RSxx, where xx is the number of the reference profile). Tug operating modes, vessel and control system parameters are detailed in [9], [10], whereas the proposed EMS parameters are summarized in TABLE I, in which $E_{SM,n}$ is the rated SM energy content. In particular, τ_1 and τ_2 have been initially set to charge/discharge SM by approximately 15% and 65% when $P_m^* = P_{m,n}$, and then tuned during simulations. Differently, $\tilde{k}$ has been set from $2/\tau_1$ to $4/\tau_1$ to speed up the E_{SM}^* tracking properly. Simulations concern also the baseline EMS of the IEEE MVC 2025, which serves as a benchmark. Notably, a time-scaling factor is applied, where one second of simulation corresponds to one minute in real-time operation, significantly reducing computational effort, while preserving accuracy.

Simulation results related to the *RS03* speed profile are presented from Fig. 4 to Fig. 8. Particularly, Fig. 4 compares the reference and actual speeds of the tug under both base and proposed EMSs during transit and assist operations (the latter approximately occurring on 30–60 s and 130–180 s). While the reference speed is perfectly tracked during transit, the tug exhibits slower acceleration during assist operations due to the increased mass and resistive force due to the towed vessel. This behaviour is consistent for both EMSs, as their actual speeds, tractive forces, and torques overlap to each other, demonstrating that control system operations are not affected by the EMS. The EMS performance is further analysed in Fig. 5 and Fig. 6, which depict the DTP-PMSM, BP and SM power distribution achieved by the proposed and the baseline EMS, respectively. Although P_e evolutions are similar, differences emerge in ΔP_e during high-power demand (i.e. P_e close or above 1 pu), due to the different SM exploitation strategies. Specifically, during the first assist interval (~30–60 s), the proposed EMS prioritizes SM for peak shaving rather than fully compensating for abrupt BP current variations. In contrast, the baseline EMS exhibits higher SM power peaks and faster discharge rates, as it lacks the dual capability of the proposed EMS to support BP during both dynamic and high-power operations. The peak-shaving capability of the proposed EMS is further demonstrated during the second assist interval (~130–180 s), where the SM provides a significant BP power reduction until the tug's acceleration ends. The evolutions of BP state-of-charge and SM state-of-energy shown in Fig. 7 and Fig. 8 confirm all these considerations, revealing a better SM exploitation provided by the proposed EMS.

The improved capability of the proposed EMS against the baseline is also confirmed by the overall cost function and its components, as summed up in TABLE II. The proposed EMS

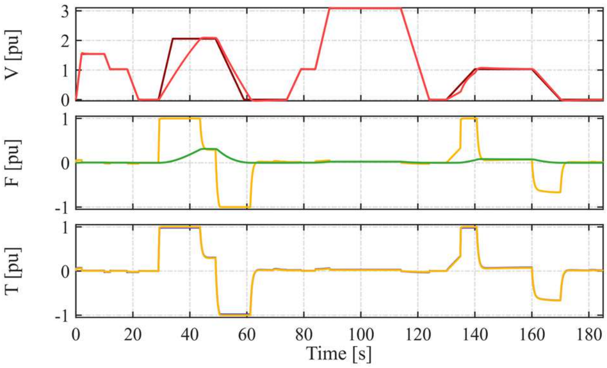

Fig. 4. Evolution of v^* (dark red) and v (pale red) profiles (on the top), F_r (green) and F_p (yellow) profiles (in the middle), T_e (yellow) and T_p (blue) profiles (on the bottom), achieved by both base and proposed EMSs.

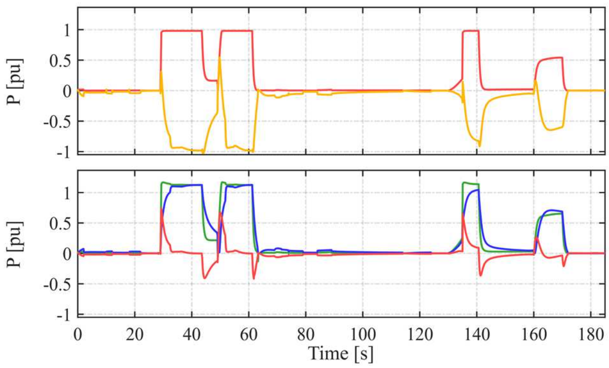

Fig. 5. Evolutions of P_e (red) and ΔP_e (yellow) on the top, P_{BP} (blue), P_{SC} (red), and $P_{BP}+P_{SM}$ (green) on the bottom, achieved by the proposed EMS.

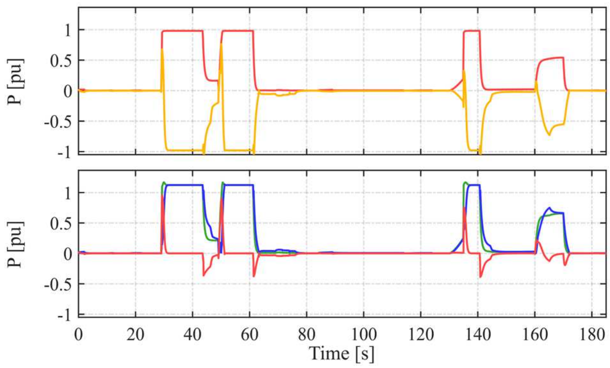

Fig. 6. Evolutions of P_e (red) and ΔP_e (yellow) on the top, P_{BP} (blue), P_{SC} (red), and $P_{BP}+P_{SM}$ (green) on the bottom, achieved by the baseline EMS.

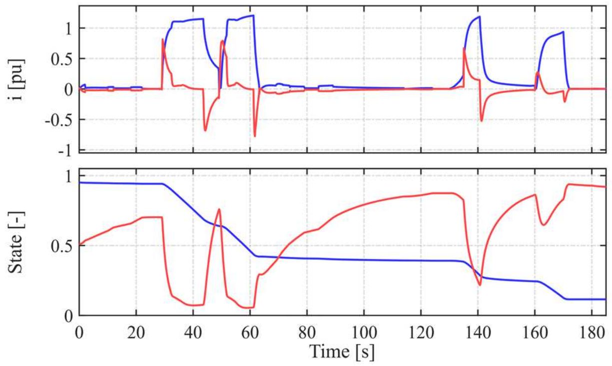

Fig. 7. Evolutions of BP (blue) and SM (red) currents (on the top), and state-of-charge/-energy (on the bottom) achieved by the proposed EMS.

TABLE II COST FUNCTION COMPONENTS ACHIEVED OVER *RS03*

Cost	Unit	Proposed EMS	Baseline EMS
$k_{BP}\,\phi_{BP}$	-	20.509	22.768
$k_E\,\phi_E$	-	18.456	17.790
$k_{SPM}\,\phi_{SPM}$	-	15.429	20.602
$k_w\,\phi_w$	-	5.573	6.095
ϕ	-	59.967	67.254

TABLE III COST FUNCTION OVER ALL IEEE MVC 2025 CYCLES

Cycle	Duration	Proposed EMS	Baseline EMS
RS00	165 s	63.415	71.212
RS01	100 s	5.398	5.086
RS02	113 s	94.425	117.760
RS03	185 s	59.967	67.254
MVC 2025 Score	-	100.530	109.409

demonstrates superior performance compared to the baseline EMS, achieving a total score of 59.967 vs 67.254. A key improvement is the nearly 25% reduction in the cost term associated with high-power operation (ϕ_{SPM}), contributing to the overall cost reduction of approximately 10.8%.

In conclusion, TABLE III compares the cost function values achieved by the proposed EMS and the baseline EMS across all the four scoring cycles used in the IEEE MVC 2025. The proposed EMS demonstrates superior performance in all cases except in *RS01*. This particular cycle is relatively short compared to the others (100 s vs 165, 113 and 185 s), and the absence of any assist operating mode results in peak power demands significantly below 1 pu, preventing the proposed EMS from effectively utilizing its peak-shaving capabilities. For the remaining three reference cycles, the proposed EMS achieves consistent performance improvements, reducing costs by over 10% in each case. Most notably, the MVC 2025 score shows an overall 8% reduction, confirming the effectiveness of the proposed approach under typical tugboat operating conditions.

V. CONCLUSIONS

An Energy Management System (EMS) for the electric propulsion system promoted by the IEEE Motor Vehicle Challenge 2025 is presented in this paper. It consists of a rule-based EMS that exploits the supercapacitor module to support the battery pack at both dynamic and high-power operations. The effectiveness of the proposed EMS has been verified by simulations, revealing a significant performance improvement compared to the baseline EMS. Further refinements can be introduced, among which a better split criterion to increase and/or extend peak-shaving capability. This and other aspects will be addressed in future works.

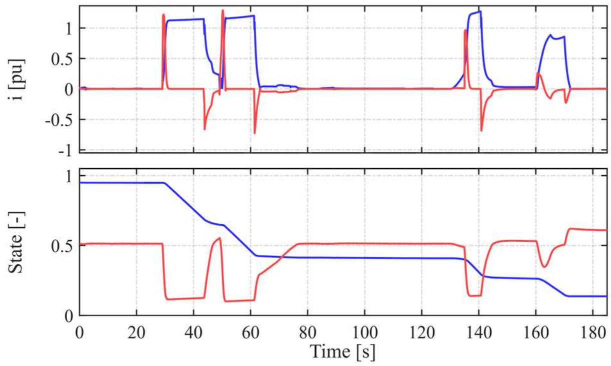

Fig. 8. Evolutions of BP (blue) and SM (red) currents (on the top), and state-of-charge/-energy (on the bottom) achieved by the baseline EMS.

ACKNOWLEDGMENT

This work is partially developed within the project NEPTUNE (Highly-iNtegrated all-Electric Propulsion-charging system on zero-emissions TUgboats for NExt-generation harbours, CUP F53D23000710006), funded by MUR under the call PNRR_M4.C2.1.1_PRIN_2022, cod. 2022RFS73J

REFERENCES

[1] M. Kolodziejski and I. Michalska-Pozoga, “Battery Energy Storage Systems in Ships’ Hybrid/Electric Propulsion Systems,” *Energies*, vol. 16, no. 3, Art. no. 3, Jan. 2023, doi: 10.3390/en16031122.

[2] S. Fang, Y. Xu, Z. Li, T. Zhao, and H. Wang, “Two-Step Multi-Objective Management of Hybrid Energy Storage System in All-Electric Ship Microgrids,” *IEEE Transactions on Vehicular Technology*, vol. 68, no. 4, pp. 3361–3373, Apr. 2019, doi: 10.1109/TVT.2019.2898461.

[3] J. Han, J.-F. Charpentier, and T. Tang, “An Energy Management System of a Fuel Cell/Battery Hybrid Boat,” *Energies*, vol. 7, no. 5, Art. no. 5, May 2014, doi: 10.3390/en7052799.

[4] N.-D. Nguyen, C. Yoon, and Y. I. Lee, “A Standalone Energy Management System of Battery/Supercapacitor Hybrid Energy Storage System for Electric Vehicles Using Model Predictive Control,” *IEEE Transactions on Industrial Electronics*, vol. 70, no. 5, pp. 5104–5114, May 2023, doi: 10.1109/TIE.2022.3186369.

[5] T. Q. Dinh, T. M. N. Bui, J. Marco, C. Watts, and J. I. Yoon, “Optimal Energy Management for Hybrid Electric Dynamic Positioning Vessels,” *IFAC-PapersOnLine*, vol. 51, no. 29, pp. 98–103, Jan. 2018, doi: 10.1016/j.ifacol.2018.09.476.

[6] R. A. Barrera-Cardenas, S. D’Arco, L. Piegari, and P. Tricoli, “Pareto-Based Design Optimisation of Hybrid Energy Storage Systems for Full-Electric Vessels,” *IET Power Electronics*, vol. 18, no. 1, p. e70027, 2025, doi: 10.1049/pel2.70027.

[7] B. Hu, Y. Xiao, S. Zhang, and B. Liu, “A Data-Driven Solution for Energy Management Strategy of Hybrid Electric Vehicles Based on Uncertainty-Aware Model-Based Offline Reinforcement Learning,” *IEEE Transactions on Industrial Informatics*, vol. 19, no. 6, pp. 7709–7719, Jun. 2023, doi: 10.1109/TII.2022.3213026.

[8] Y. Mazzi, H. Ben Sassi, F. Errahimi, and N. Es-Sbai, “A soft actor-critic reinforcement learning framework for optimal energy management in electric vehicles with hybrid storage,” *Journal of Energy Storage*, vol. 99, p. 113344, Oct. 2024, doi: 10.1016/j.est.2024.113344.

[9] M. Porru, A. Serpi, F. Tinazzi, and L. Ortombina, “IEEE VTS Motor Vehicle Challenge 2025 – Energy Management and Control of a Marine Electric Propulsion System,” in *Proc. of 2024 IEEE Vehicle Power and Propulsion Conference (VPPC 2024)*, Washington DC (USA), Oct. 2024, pp. 1–6. doi: 10.1109/VPPC63154.2024.10755298.

[10] A. Serpi, M. Porru, A. Turno, F. Tinazzi, M. Pastura, and M. Zigliotto, “Asymmetric Supply of a Dual Three-Phase PMSM through a Hybrid Energy Storage System in Marine Electric Propulsion Systems,” in *Proc. of 2024 IEEE Vehicle Power and Propulsion Conference (VPPC 2024)*, Washington DC (USA), Oct. 2024, pp. 1–6. doi: 10.1109/VPPC63154.2024.10755331.

[11] J. Carlton, *Marine Propellers and Propulsion, Second Edition*. Butterworth-Heinemann, 2012.